



Contents lists available at ScienceDirect

# Mechanical Systems and Signal Processing

journal homepage: [www.elsevier.com/locate/ymssp](http://www.elsevier.com/locate/ymssp)



## Phase-based time domain averaging (PTDA) for fault detection of a gearbox in an industrial robot using vibration signals

Yunhan Kim <sup>a</sup>, Jungho Park <sup>c</sup>, Kyumin Na <sup>a</sup>, Hao Yuan <sup>a</sup>, Byeng D. Youn <sup>a,b,c,\*</sup>, Chang-soon Kang <sup>d</sup>

<sup>a</sup> Department of Mechanical and Aerospace Engineering, Seoul National University, Seoul 08826, Republic of Korea

<sup>b</sup> Institute of Advanced Machines and Design, Seoul National University, Seoul 08826, Republic of Korea

<sup>c</sup> OnePredict Inc., Seoul 08826, Republic of Korea

<sup>d</sup> Robot Research Institute, Hyundai Heavy Industries Holdings Co., Ltd., Gyeonggi-do 16891, Republic of Korea



### ARTICLE INFO

#### Article history:

Received 29 May 2019

Received in revised form 2 October 2019

Accepted 24 November 2019

Available online 12 December 2019

#### Keywords:

Industrial robot

Gearbox

Fault detection

Vibration signal

Time domain averaging (TDA)

### ABSTRACT

This paper proposes a fault detection method that uses vibration signals in the gearboxes of industrial robots. The vibration signals from gearboxes consist of both deterministic signals and residual signals; fault-related signals usually exist in the residual signals. Previously, *time domain averaging* (TDA) has been studied to derive the deterministic signals. However, the performance of TDA method is limited when the signals are poorly synchronized. Therefore, we propose a new *phase-based time domain averaging* (PTDA) method. The proposed PTDA method can estimate deterministic signals that are more synchronized by considering the phase angle of the vibration signals. Then, the residual signals can be calculated by subtracting the estimated deterministic signals from the measured vibration signals using the PTDA method. We use two health features, root-mean-square (RMS) and power spectrum entropy, to quantify the fault severity in the residual signals. To demonstrate the proposed method, we use vibration signals measured from a six-degree-of-freedom (6-DOF) industrial robot test-bed under 1) a simple one-joint rotating motion, 2) a complicated arc welding motion, and 3) a spot welding motion. The results show that the proposed PTDA method can improve the performance of fault detection for gearboxes in industrial robots.

© 2019 Elsevier Ltd. All rights reserved.

## 1. Introduction

Industrial robots are key manufacturing equipment and have been gaining widespread use in various industries, such as aerospace and automotive [1,2]. The global supply of industrial robots has been growing in recent years by 10%, to 421,000 units in 2018; the number of in-service industrial robots is expected to increase by an average 14% per year to reach 630,000 units in 2021 [3]. Since many industrial robots are placed and operated in manufacturing lines to improve work efficiency and the quality of the products [2,4], failure of any industrial robot could increase downtime of the manufacturing process and cause huge economic loss [5]. To minimize downtime loss, condition monitoring and fault detection techniques for industrial robots have recently been extensively investigated.

Freyermuth [6] proposed a model-based approach to detect incipient faults in industrial robots. In this approach, control signals were used to estimate the friction coefficients in the joint of the robot and the fault was detected based on these

\* Corresponding author at: Department of Mechanical and Aerospace Engineering, Seoul National University, Seoul 08826, Republic of Korea.

E-mail addresses: [yunhan.kim91@gmail.com](mailto:yunhan.kim91@gmail.com) (Y. Kim), [bdyoun@snu.ac.kr](mailto:bdyoun@snu.ac.kr) (B.D. Youn).

estimated coefficients. Capisani et al. [7] also proposed a model-based technique to detect actuator faults in an industrial robot. However, these model-based methods have limitations because it is not easy to construct and validate a dynamic model of a robot [8]. Pan et al. [9] detected the backlash fault of a joint in an industrial robot using vibration signals. The health features were simply extracted using the Wigner-Vile distribution (WVD) of the vibration signals and the features were used as inputs for the artificial neural network (ANN) algorithm. Jaber and Bicker [10] developed a fault diagnosis algorithm for backlash of the gearbox in an industrial robot joint. In the proposed algorithm, the vibration signals were decomposed using discrete wavelet transform (DWT), and simple statistical features of the decomposed signals were used as inputs for the ANN algorithm. Datta et al. [11] also used the coefficients of DWT as the health features and the ANN algorithm as the classifier. The method was validated with six different fault conditions using a four-degree-of-freedom (4-DOF) robot arm from the semiconductor industry. These studies show that the ANN algorithm is effective in classifying the conditions of an industrial robot using simple health features derived from WVD and/or DWT. However, the ANN algorithm usually requires huge datasets of normal and fault conditions to enable sufficient training of the fault diagnosis algorithm with the health features. Recently, there have been some studies to evaluate the condition of industrial robots based on accuracy degradation. Quao and Weiss [12] proposed an advanced sensing technique with a seven-dimensional measurement system to assess the accuracy degradation of an industrial robot. To et al. [13] proposed a real-time fault detection method using multiple sensors, including red, green, blue-depth (RGB-D) camera, audio, and pressure transducers. In this method, a fault was detected based on the discrepancy between the sensed and expected working positions. The proposed method was validated with an industrial robot in a grit-blasting operation. Although a fault in an industrial robot could be detected based on the working performance, this method could not determine which component was in a faulty state. Therefore, component-level fault detection techniques are still needed to identify the root cause of the fault and enable proper maintenance action on the degraded component.

In this study, we propose a new method to develop sensitive features for detecting faults in industrial robots. While some industrial robots perform a variety of job tasks, others perform only one repetitive task. We limited the scope of this study to development of a fault detection method for industrial robots that perform the same job task repeatedly. Since the gearbox transmits the torque directly to the joint, the gearbox significantly affects the performance of the industrial robot. Therefore, we focus on a method of fault detection for gearboxes used in industrial robots. In addition, we use the vibration signal for fault detection, which is known as one sensitive signal that can be used to detect a fault of a gearbox [14–21]. In general, the vibration signals from a gearbox comprise both deterministic signals and residual signals [22]. The deterministic signals originate from the periodic excitation of the components in the gearbox. On the other hand, the residual signals include noises and fault-related signals. Since fault-related signals usually exist in the residual signals, many fault detection methods have been developed to obtain residual signals from the measured vibration signals. In the proposed method, we exploit a time domain averaging (TDA) method to extract the deterministic signals [23] and enhance the fault-related signals by subtracting the deterministic signals from the raw signals. However, the previous TDA method could extract inaccurate deterministic signals when the target signals were not perfectly synchronized. Therefore, in the proposed method, we consider the phase angle of the vibration signals for the TDA method. We call this new method phase-based time domain averaging (PTDA). In the proposed method, we first extract raw vibration signals based on the constant angular speed region. This step is performed to reduce the variability of the vibration signals that arises from the complex motions of the industrial robot. In the second step, we estimate the deterministic signals by using the extracted raw vibration signals and applying the PTDA method. This step is used to estimate deterministic signals, which are more synchronized with the extracted raw signals at each cycle due to the use of the same phase angle. Then, as the third step, the residual signals are calculated by subtracting the estimated deterministic signals from the extracted raw signals. This step enhances the fault-related signals because the residual signals are more sensitive to faults than the raw signals [24,25]. In the last step, we calculate health features based on the residual signals to quantify the faults of the industrial robot gearbox by considering the characteristics of the residual signals.

This paper is organized as follows. Section 2 describes the general configuration and vibration signals of a gearbox in an industrial robot. Section 3 explains in detail the proposed method, PTDA, to detect a fault of a gearbox used in an industrial robot. Section 4 validates the proposed method through the use of three case studies: the first examines an industrial robot under a simple rotating motion; the second examines a complicated motion (i.e., arc welding); the third examines a spot welding motion that is common in the automotive industry. Finally, Section 5 provides a conclusion and suggestions for future work.

## 2. Background: The industrial robot and vibration signals from the gearbox

In this section, we describe background knowledge about industrial robots and about gearbox vibration signals in industrial robots. First, we explain the configuration and basic principles of the working path in the industrial robot. Then, we investigate the composition of gearbox vibration signals in industrial robots.

### 2.1. Configuration of industrial robots

Industrial robots are kinematically composed of links and joints that, together, allow the robot to generate complex motions. The number of DOFs in an industrial robot is equal to the number of joints [2]; typical industrial robots have 6 DOFs,

which allows them to conduct specified tasks by imitating the motion of a human arm [10,26,27]. The typical configuration of an industrial robot is shown in Fig. 1. To conduct its required tasks, an industrial robot requires the working path of six joints. The working path of each joint is generated with several via points and is segmented by two successive via points. Several methods are available to define the shape of the working path segment as functions with respect to the joint's rotating angles. In this study, we apply a linear function with parabolic blends for path shape method [2], where the joint accelerates from the previous via point, rotates with a constant angular speed, and decelerates to the next via point. Fig. 2 shows examples of the working path, via points, angular speed, and angle profile at the 4th joint. For the purpose of control, the angle and/or the angular speed profiles of the joints can be acquired from the robot's controller [8].

In order to generate the working path while joints are rotating, driving systems are required for industrial robots. The most common driving system includes an actuator and a transmission system. An electric motor is widely used as the actuator, and a gearbox is generally used as the transmission system [2,28]. Industrial robots require the torque of the joints to follow the working path. The electric motor is driven at high speed and low torque, and the gearbox reduces the speed of the motor to transmit the required large torque to the joint of the robot [29]. Then, each joint rotates along the working path with the rotating of the gearbox and, finally, the industrial robot is able to execute specified tasks, such as welding, precision assembly, packaging, and labeling [26,30].

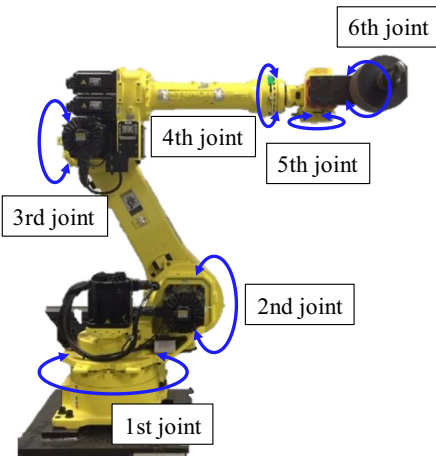


**Fig. 1.** Configuration of a 6-DOF industrial robot.

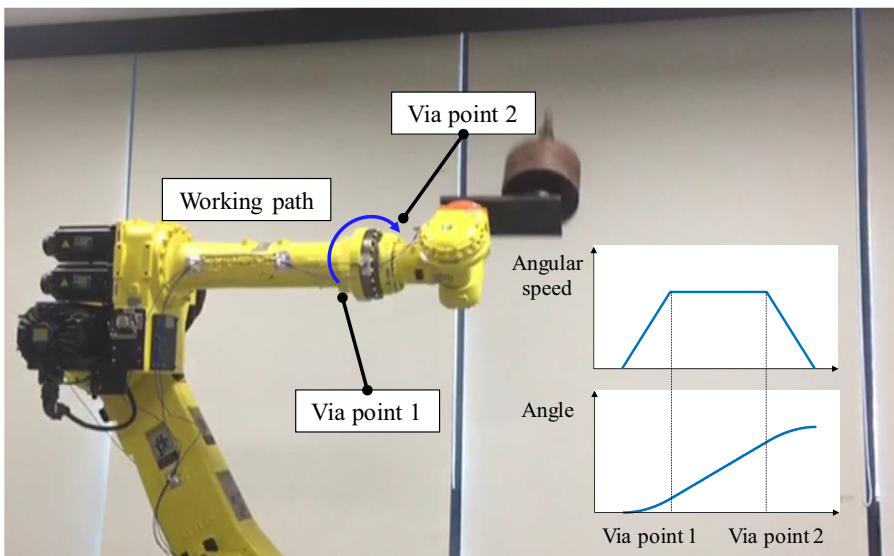


**Fig. 2.** Examples of the working path, via points, angular speed and the angle profile at the 4th joint.

## 2.2. Characteristics of the vibration signals of gearboxes used in industrial robots

As noted in [Section 1](#), we use vibration signals for fault detection of a robot's gearbox. The gearbox works as the transmission system in an industrial robot. A cycloidal gearbox is widely used in industrial robots for transmitting high torque due to the high transmission ratio of this type of gearbox [31,32]. [Fig. 3](#) shows the components of a cycloidal gearbox in an industrial robot, which include an input gear, spur gears, a cycloidal disk, and pins. As shown in [Fig. 3\(a\)](#), the input gear is linked to the motor through an input shaft. There are two transmission stages in a cycloidal gearbox. At the first stage, the input gear and input shaft rotate the spur gears, which are shown in [Fig. 3\(b\)](#). At the second stage, the shafts linked to the three spur gears drive the cycloidal disk in an eccentric motion, which mates the pins, as shown in [Fig. 3\(c\)](#). Therefore, a cycloidal gearbox can achieve a high transmission ratio, which is expressed as

$$R = 1 + \frac{Z_{\text{spur}}}{Z_{\text{in}}} Z_{\text{pin}} \quad (1)$$

where  $Z_{\text{in}}$  is the number of teeth on the input gear,  $Z_{\text{spur}}$  is the number of teeth on the spur gear, and  $Z_{\text{pin}}$  is the number of pins.

The vibration signal from a cycloidal gearbox,  $x[n]$ , can be divided into a deterministic signal and a residual signal, which can be expressed as

$$x[n] = d[n] + r[n] \quad (2)$$

where  $n$  is discrete time,  $d[n]$  is the deterministic signal, and  $r[n]$  is the residual signal. The deterministic signals typically originate from excitation of periodic motions in gearbox components, such as gear tooth meshing [22,33]. The residual signals are mainly from sources other than the sources of the deterministic signals, for example, noises and faulty signals [22]. For traditional gearboxes, such as spur gearboxes and planetary gearboxes, the source of the deterministic signals is the periodic meshing of gear teeth in the gearboxes. In a cycloidal gearbox, there are two main excitation sources, meshing between the input gear and the spur gear, and between the cycloidal disk and the pins. The fundamental frequency that arises from the meshing of the input gear and the spur gear is called a gear mesh frequency (GMF). Likewise, the fundamental frequency that arises from the meshing of the cycloidal disk and the pins is called a disk mesh frequency (DMF). The GMF and DMF can be calculated as

$$\text{GMF} = Z_{\text{in}} f_{\text{in}} \quad (3)$$

$$\text{DMF} = Z_{\text{pin}} f_{\text{out}} \quad (4)$$

where  $Z_{\text{in}}$  is the number of teeth on the input gear,  $Z_{\text{pin}}$  is the number of pins, and  $f_{\text{in}}$  and  $f_{\text{out}}$  are the input and output shaft speed, respectively. In industrial robots, the input shaft speed is equal to the motor angular speed and the output shaft speed is matched with the joint angular speed. Due to the high transmission ratio of a cycloidal gearbox, the DMF is located in the low-frequency region. In general, the magnitudes at the DMF and its harmonics from the gearbox are imperceptible from the noises in the low-frequency region [34]. However, the magnitudes at the GMF and its harmonics are relatively large in the frequency domain. Therefore, the deterministic signals from a cycloidal gearbox include the large magnitudes at the characteristic frequencies of the gearbox from GMF and its harmonics in the frequency domain.

The vibration signals in a normal condition include the deterministic signals and the noises. Thus, the residual signals usually consist of the noises. However, the vibration signals in a fault condition include the deterministic signals, the noises, and the fault-related signals. Therefore, the residual signals in the fault condition contain both the noises and the fault-related signals. In general, it is challenging to identify the fault only using the raw vibration signals because the deterministic signals take up a large portion of the measured vibration signals. Thus, many studies have focused on using the residual

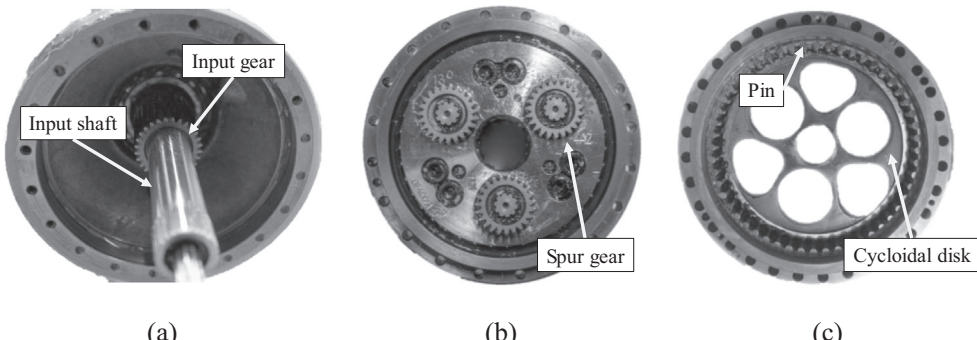


**Fig. 3.** Components of the cycloidal gearbox in an industrial robot: (a) input gear and input shaft, (b) spur gears, (c) cycloidal disk and pin.

signals for early fault detection [24,25] by removing the deterministic signals from the raw vibration signals. Through this process, fault-related signals could be highlighted in the residual signals. However, the residual signals may be calculated inaccurately when the measured vibration signals are poorly synchronized.

### 3. Proposed phase-based time domain averaging (PTDA) method for fault detection of a gearbox in an industrial robot

In this section, we describe the proposed PTDA method in detail. The proposed method intends to derive the residual signals more accurately to obtain features that are sensitive to the fault. A summary of the proposed method is presented in Fig. 4. The detailed procedures of the method are described in this section.

#### 3.1. Signal extraction in the constant angular speed region

The proposed method is based on vibration signals. The vibration signals can be measured using external transducers attached to a gearbox, such as accelerometers. In addition, the angular speeds are measured using data from the robot's controller. As described in Section 2.1, a typical angular speed profile consists of the accelerating region from the initial position, the constant angular speed region, and the decelerating region toward the end position [9]. Since the characteristic frequencies of a gearbox are proportional to the gearbox shaft speed, as described in Section 2.2, the characteristic frequencies also increase, have the constant values, and decrease over time. Therefore, we first extract the raw signals within the constant angular speed region with the same direction by using the joint angular speed. This step could reduce the variability of the characteristic frequencies for the measured vibration signals. Then, the extracted raw signals under constant speed regions would have constant characteristic frequencies over the signals.

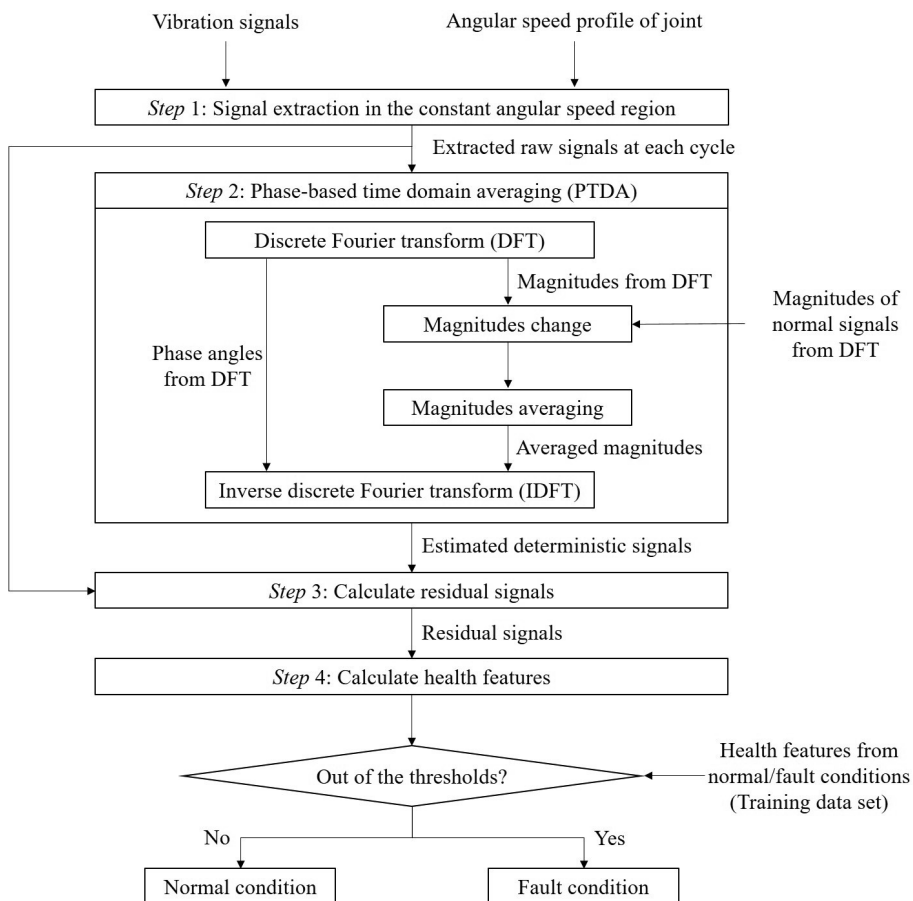


**Fig. 4.** Flowchart of the proposed method.

### 3.2. Phase-based time domain averaging (PTDA)

The extracted raw signals have constant characteristic frequencies due to the constant angular speed of the gearbox. As described in [Section 2.2](#), the vibration signals of the cycloidal gearbox consist of both deterministic and residual signals [\[22\]](#). The deterministic signals can be commonly observed in both normal and fault conditions. However, the residual signals are more significant in the fault condition than in the normal condition because the residual signals can contain fault-related signals. Therefore, the fault-related signals in the measured vibration signals could be highlighted by eliminating the deterministic signals. The deterministic signals,  $d[n]$ , can be obtained by the TDA method, as

$$d[n] = \frac{1}{M} \sum_{i=1}^M x_i[n] \quad (5)$$

where  $x_i[n]$  is the  $i$ th extracted raw signal from [Step 1](#), and  $M$  is the total number of cycles. The basic assumption of the TDA method is that the extracted raw signals are perfectly synchronized in the time domain. However, the extracted raw signals are not perfectly synchronized due to phase differences among signals at each cycle.

To solve this problem of the TDA method, we propose a phase-based time domain averaging (PTDA) method. The PTDA method can estimate the synchronized deterministic signals at each cycle by considering the phase angle of the vibration signals. We can obtain the phase angle of the signals by using a discrete Fourier transform (DFT), which means Fourier representation of the discrete signal. DFT is applied to the extracted raw signals; this process is expressed as

$$X_i[k] = \sum_{n=0}^{N-1} x_i[n] e^{-j(2\pi/N)kn} = |X_i[k]| e^{j\theta_i[k]} \quad (6)$$

where  $k$  is the discrete frequency,  $X_i[k]$  is the DFT of the  $i$ th extracted signal,  $|X_i[k]|$  is the magnitude and  $\theta_i[k]$  is the phase angle of the extracted raw signal [\[35\]](#). In practice, a fast Fourier transform (FFT) algorithm can be used to improve the computational efficiency of the DFT. Although the extracted raw signals are not perfectly synchronized in the time domain, the magnitude of the DFT is synchronized in the frequency domain due to the use of the same characteristic frequencies from the constant angular speed of the gearbox. The magnitude of the extracted raw signal contains both the deterministic components and the residual components. Then, the average magnitude from the extracted signals for the normal condition results in the deterministic components of the signal in the frequency domain. The average magnitude is calculated with the magnitudes of the DFTs as

$$|D_{avg}[k]| = \frac{1}{M} \sum_{i=1}^M |X_i[k]| \quad (7)$$

To estimate the deterministic signals in the time domain, the inverse DFT (IDFT) is used with the average magnitude  $|D_{avg}[k]|$  and the phase angle  $\theta_i[k]$  at each cycle, as follows:

$$D_i[k] = |D_{avg}[k]| e^{j\theta_i[k]} \quad (8)$$

$$d_i[n] = \frac{1}{N} \sum_{k=0}^{N-1} D_i[k] e^{j(2\pi/N)kn} \quad (9)$$

where  $D_i[k]$  is the DFT of the  $i$ th estimated deterministic signal, and  $d_i[n]$  is the estimated deterministic signal at each cycle in the time domain, which is the IDFT of  $D_i[k]$ . Using the above procedure, we can obtain the estimated deterministic signals at each cycle, which are synchronized with each extracted raw signal in the time domain.

[Fig. 5](#) shows a comparison of the TDA and PTDA methods for 10 cycles of simulated signals with a gear mesh frequency (GMF) of 520 Hz and with different phase angles. One simulated signal can be expressed as

$$x[n] = \sum_{k=1,4,5,7,8,12} A_k \sin(2\pi k f_{GMF}(n + \theta_k)) + w[n] \quad (10)$$

where  $f_{GMF}$  is the GMF,  $w[n]$  is the noise signal, and  $A_k$  and  $\theta_k$  are the amplitude and the phase angle of  $k$ th harmonic signal, respectively. The amplitudes are shown in [Table 1](#). The phase angles,  $\theta_k$ , for each simulated signal can be arbitrarily selected to simulate signals with different phase angles. In this case, we randomly selected the values of the phase angles to be between zero and one. In addition, we set the signal-to-noise ratio (SNR) to  $-10$  dB for the noise signals. [Fig. 5\(a\)](#) shows one simulated signal in the time and frequency domains. [Fig. 5\(b\)](#) shows the estimated deterministic signals from 10 cycles of simulated signals using the TDA method in the time and frequency domains. As shown in [Fig. 5\(b\)](#), the magnitudes of the GMF and its harmonics derived from the TDA method are less than the magnitudes of the GMF and its harmonics from the simulated signal in [Fig. 5\(a\)](#). This is because the 10 cycles of simulated signals have phase differences; thus, we could not estimate deterministic signals perfectly. [Fig. 5\(c\)](#) shows the estimated deterministic signals from the PTDA method in the time and frequency domains. As shown in [Fig. 5\(c\)](#), we found that the magnitudes of the signals in the time and frequency

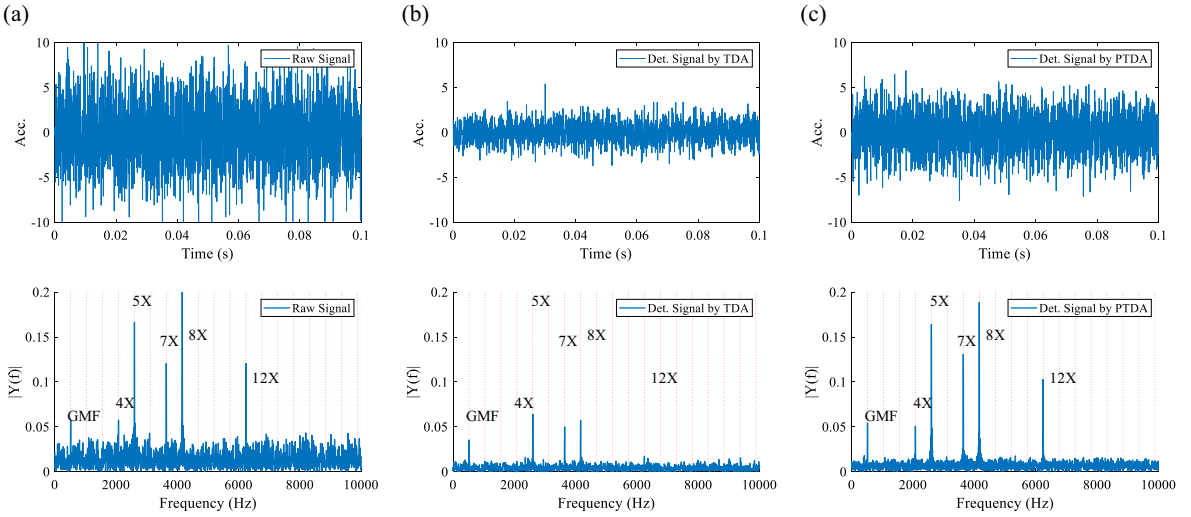


**Fig. 5.** Comparison of TDA and PTDA: (a) simulated signal, (b) deterministic signal found by TDA, (c) deterministic signal found by PTDA in the time (upper row) and frequency (lower row) domains.

**Table 1**  
Amplitudes of the simulated signals.

Parameter	$A_1$	$A_4$	$A_5$	$A_7$	$A_8$	$A_{12}$
Value	0.43	0.48	1.40	1.10	1.60	0.94

domains are as large as the ones from the one simulated signal shown in Fig. 5(a). Therefore, we found that the estimated deterministic signals derived from the PTDA method could better represent the deterministic signals than the TDA method.

### 3.3. Residual signal calculation

As noted in Section 2.2, the residual signals contain the faulty information of the vibration signals in the gearbox. Therefore, in this step, we calculate the residual signals using the extracted raw signals from Step 1 and the estimated deterministic signals from Step 2. In normal conditions, the residual signals can be derived by subtracting the estimated deterministic signals from the extracted raw signals. This is true because the estimated deterministic signals and the extracted raw signals are synchronized. The residual signals are expressed as follows

$$r_i[n] = x_i[n] - d_i[n] \quad (11)$$

where  $r_i[n]$  is the  $i$ th residual signal,  $x_i[n]$  is the  $i$ th extracted raw signal, and  $d_i[n]$  is the  $i$ th deterministic signal found by the PTDA method.

However, the magnitudes of the fault signals include the magnitudes of both the deterministic signals and the fault-related signals. Thus, the deterministic signals from the fault signals are estimated with the magnitudes of the normal signals and the phase angle of the fault signals using the PTDA method as follows.

$$D_{i,fault}[k] = |D_{avg,normal}[k]| e^{j\theta_{i,fault}[k]} \quad (12)$$

$$d_{i,fault}[n] = \frac{1}{N} \sum_{k=0}^{N-1} D_{i,fault}[k] e^{j(2\pi/N)kn} \quad (13)$$

where  $\theta_{i,fault}[k]$  is the phase angle of the DFT with the  $i$ th fault signal. These signals could represent the deterministic signals without the fault-related signals. Then, the residual signals can be derived in the same manner as for the normal condition, by subtracting the estimated deterministic signals from the extracted raw signals.

### 3.4. Health features with residual signals

To quantify the severity of the fault, we use two health features based on the residual signals: root-mean-square (RMS) in the time domain and power spectrum entropy in the frequency domain. The first feature, RMS, is used in this study to represent the energy of the residual signal in the time domain [36] and can be expressed as

$$RMS_{\text{res},i} = \sqrt{\frac{1}{N} \sum_{n=0}^{N-1} (r_i[n])^2} \quad (14)$$

where  $r_i[n]$  is the  $i$ th residual signal, and  $N$  is the length of the signal. The RMS values increase when a fault happens in the system. In addition, the RMS of the residual signal could be more sensitive to a fault than the RMS of the extracted raw signal because the power of the fault-related signals can be highlighted without the deterministic signals.

The second feature, power spectrum entropy, is used to represent the variation of the residual signal in the frequency domain [37]. A smaller entropy indicates that the data is relatively centralized, and a larger entropy indicates that the data is relatively distributed [38]. In this study, we calculate the power spectrum entropy using the spectrum of the residual signals in the frequency domain. The power spectrum entropy can be expressed as

$$\text{Entropy}_{\text{res},i} = - \sum_{k=0}^{N-1} \overline{SR}_i[k] \log(\overline{SR}_i[k]) \quad (15)$$

where  $\overline{SR}_i[k]$  is the normalized power spectrum of the residual signal in the frequency domain. Without the normalization of the power spectrum, the power spectrum entropy values could also depend on operating conditions, like angular speed and loading. Thus, in this study, we normalize the power spectrum by dividing the summation of the total power energy as follows

$$\overline{SR}_i[k] = \frac{|R_i[k]|^2}{\sum_{k=0}^{N-1} |R_i[k]|^2} \quad (16)$$

where  $R_i[k]$  is the magnitude of the residual signal in the frequency domain. As noted in [Section 2.2](#), most of the residual signals in the normal condition consist of the noises, which show that the magnitudes are distributed in the frequency domain. However, the residual signals in the fault condition include both the noises and the fault-related signals. The fault-related signals could be centralized in the specific frequency region. Therefore, we expect that the power spectrum entropy would be larger in the normal condition.

Lastly, to detect a fault based on the two health features (i.e.,  $RMS_{\text{res}}$ , and  $\text{Entropy}_{\text{res}}$ ), we carefully define their thresholds using the training data set. The proposed method is designed to detect a fault if the value of either of the two health features is out of its normal threshold value.

#### 4. Experimental validation

The proposed method was validated with experiments. In this section, we describe the industrial robot test-bed that was used to acquire the vibration signals for the experimental validation. Then, we discuss the results of the proposed method from three test cases: simple rotating motions, arc welding motions, and spot welding motions.

##### 4.1. Industrial robot test-bed setup

The proposed method was validated using a 6-DOF industrial robot test-bed with 80kgf of payload. The cycloidal gearbox was used in the joint of the industrial robot to achieve a high transmission ratio, as described in [Section 2](#). The detailed parameters of the cycloidal gearbox are described in [Table 2](#). From Eq. (1), the transmission ratio can be calculated as  $R = 33.86$ . [Fig. 6\(a\)](#) shows the overall configuration of the test-bed, and [Fig. 6\(b\)](#) shows the 4th joint that we used for our target gearbox. We used the angular speed profiles of each joint from the industrial robot, which were obtained from the robot controller, as shown in [Fig. 6\(a\)](#). We also measured the vibration signals from the joint of the industrial robot test-bed using accelerometers attached at each joint, as shown in [Fig. 6\(b\)](#). We used a faulty gearbox at the 4th joint achieved from an actual manufacturing line, which was provided from Hyundai Robotics. Next, we selected three job tasks to validate the proposed method. The first job task was the rotation of only the 4th joint of the robot. This job task is described in [Section 4.2](#). The objective of this job task is to observe the performance of the proposed method under a sufficient constant angular speed region. However, industrial robots typically work with the complicated working paths involving all joints. Therefore, the second job task was an arc welding motion used at a real manufacturing site, which consists of complex motions. The results of our proposed method under the arc welding motion are described in [Section 4.3](#). Finally, to further investigate the performance of our proposed method in real-world applications, we considered a third task, a spot welding

**Table 2**  
Detailed parameters of the cycloidal gearbox.

Parameter	Value
Number of input gear teeth, $Z_{\text{in}}$	28
Number of spur gear teeth, $Z_{\text{spur}}$	23
Number of pins, $Z_{\text{pin}}$	40

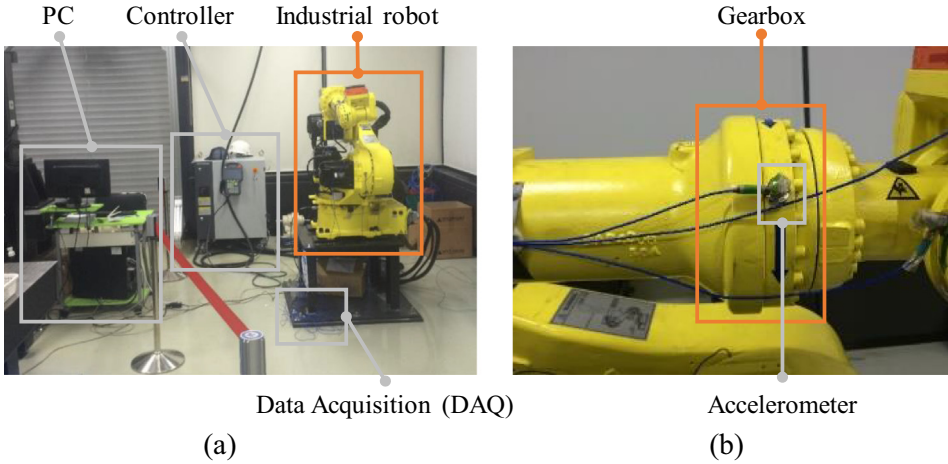


**Fig. 6.** Overall configuration of the industrial robot test-bed: (a) test-bed setup, (b) target gearbox.

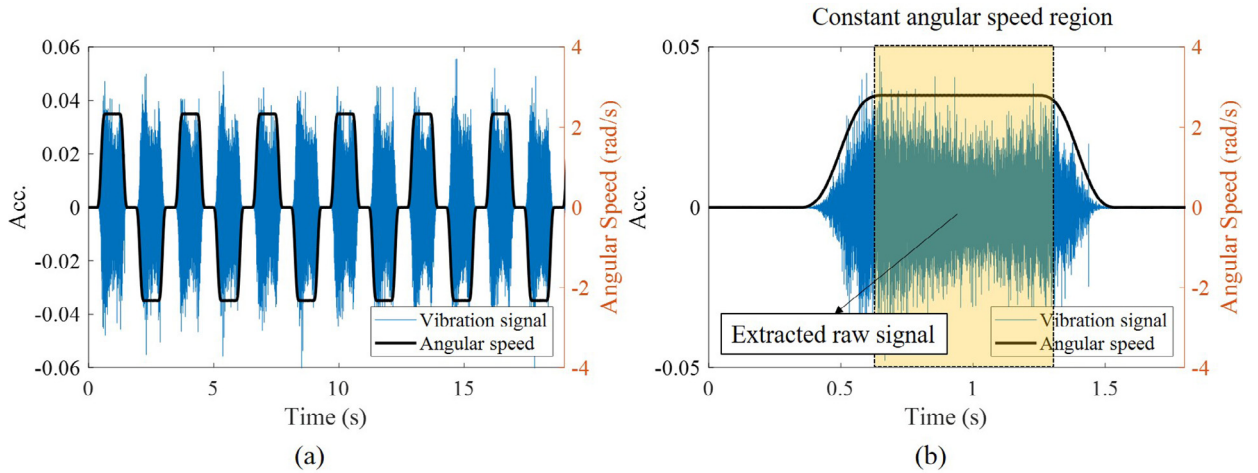


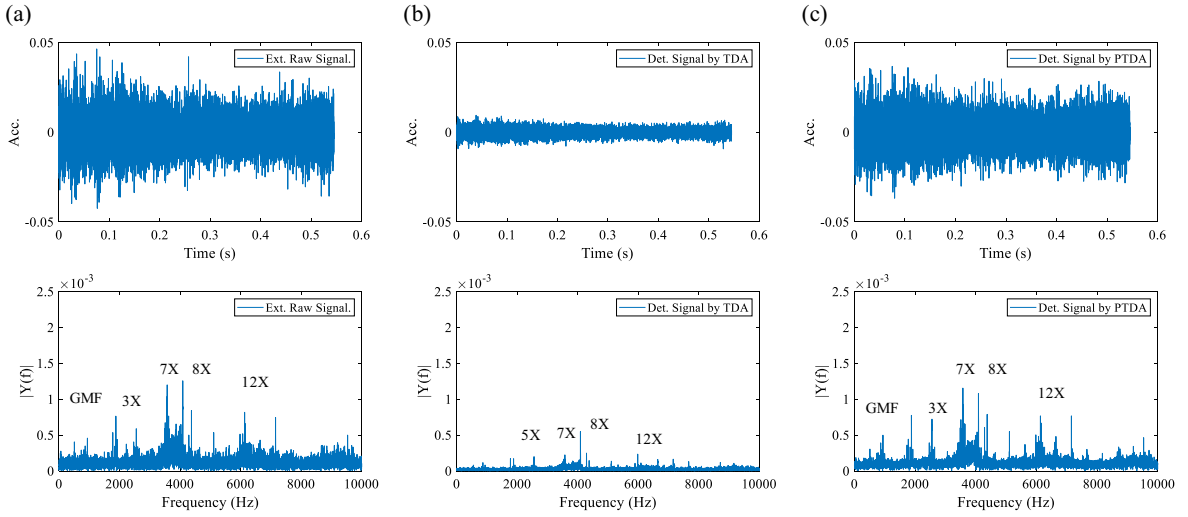
**Fig. 7.** Vibration signal and angular speed profile at the 4th joint under the 4th joint rotating motion: (a) six cycle, (b) constant angular speed region.

motion. Spot welding with industrial robots is a crucial task in the automotive industry [39]. In addition, the speed of the spot welding motion is relatively slow compared to the other two job tasks examined in the case studies. The results of our proposed method under a spot welding motion are described in Section 4.4.

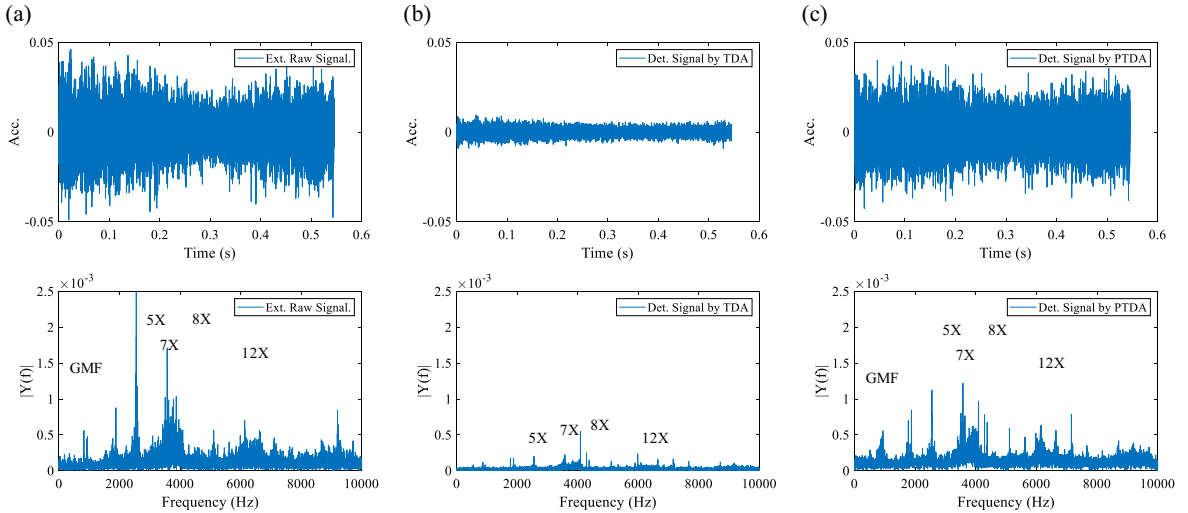
#### 4.2. Result 1: 4th joint rotating motion

Fig. 7 shows the vibration signal and the angular speed profile at the 4th joint for the rotating motion. ([The video of the experiment is available in Supplementary material](#)). The vibration signal and the angular speed profile for six cycles of the 4th joint rotating motion are shown in Fig. 7(a). The working path of the 4th joint consisted of only two via points; the joint rotates along a semicircle with a reciprocating motion. As noted in Section 2.1, the angular speed profile included the constant angular speed region between the two via points. Thus, the vibration signal of the constant angular speed region could be extracted. One of the extracted raw signals is shown in Fig. 7(b). The extracted raw signals are not synchronized because those signals have different phase angles. In this case, the output shaft speed is about 3.50 rad/s, and the time length was about 0.6 s at the constant angular speed region. Then, the GMF could be computed as 526.67 Hz using Eq. (3).

Figs. 8 and 9 show the extracted raw signals, the deterministic signals found by the TDA method, and the deterministic signals found by the proposed PTDA method under the 4th joint rotating motion in normal and faulty conditions, respectively. Based on Figs. 8(a) and 9(a), we can observe that the extracted raw signals include large magnitudes at the GMF and its harmonics in the frequency domain from the deterministic signals. In order to obtain the deterministic signals, we used the TDA and PTDA methods. Figs. 8(b) and 9(b) show the estimated deterministic signals found by the TDA method. Since the extracted raw signals could not be fully synchronized, the TDA method derived the low magnitudes at the GMF and its harmonics, which are the inaccurate deterministic signals. Figs. 8(c) and 9(c) show the estimated deterministic



**Fig. 8.** Extracted and deterministic signals in the normal condition: (a) extracted raw signal, (b) deterministic signal found by the TDA method, (c) deterministic signal found by the PTDA method.



**Fig. 9.** Extracted and deterministic signals in the fault condition: (a) extracted raw signal, (b) deterministic signal found by the TDA method, (c) deterministic signal found by the PTDA method.

signals found by the PTDA method. As described in Section 3, the PTDA method first requires normal signals to subsequently obtain the deterministic signals. In this case, the normal signals are the extracted raw signals from the robot when operating in its normal condition. One of the normal signals is shown in Fig. 8(a). Then, the PTDA method can estimate accurate deterministic signals by considering the phase angle. Thus, the estimated deterministic signals could well represent the deterministic signals, which show the large magnitudes at the GMF and its harmonics.

In addition, Figs. 10 and 11 show the residual signals obtained by the TDA and PTDA methods for normal and faulty conditions, respectively. Based on Figs. 10(a) and 11(a), we can observe that the residual signals have the deterministic components, such as GMF and its harmonics, in the frequency domain because the deterministic signals from the TDA method were not accurately removed from the raw signals. Based on Figs. 10(b) and 11(b), we can observe that the residual signals found by the PTDA method show the lower magnitudes at the GMF and its harmonics in the frequency domain because the estimated deterministic signals found by the PTDA method can be better synchronized with the extracted raw signals by considering the phase angle in the frequency domain. Then, the fault-related signals can be highlighted at the residual signals, as marked in Fig. 11(b).

Next, we calculated the health features,  $RMS_{res}$  and  $Entropy_{res}$ , from the residual signals. We compared the feature values calculated from the proposed PTDA method with the ones found from the TDA method. Fig. 12 shows the rate changes of the

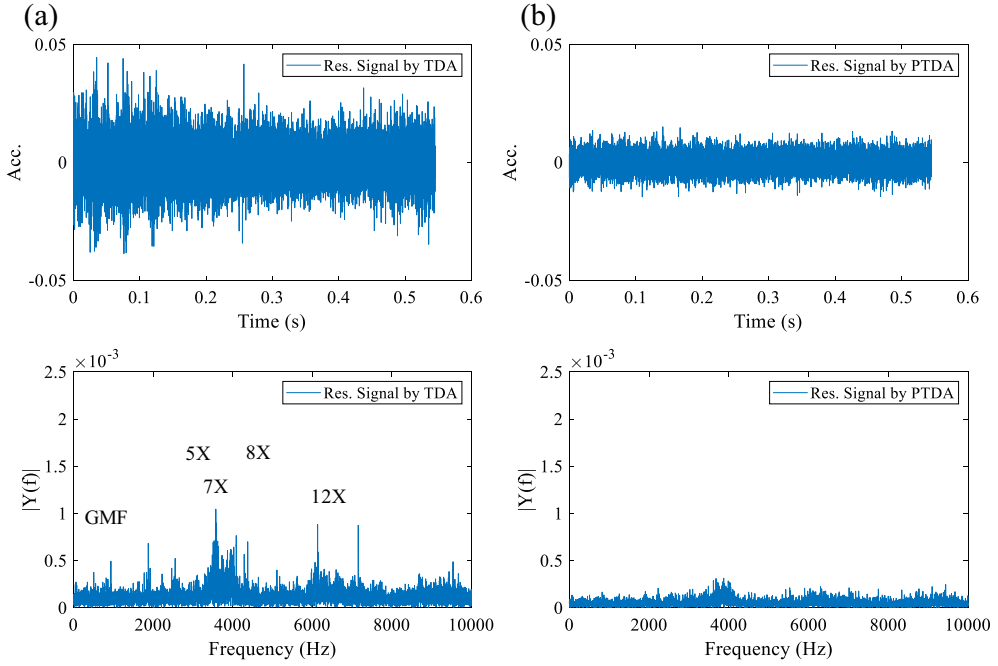


**Fig. 10.** Residual signals in the normal condition using (a) TDA and (b) PTDA.

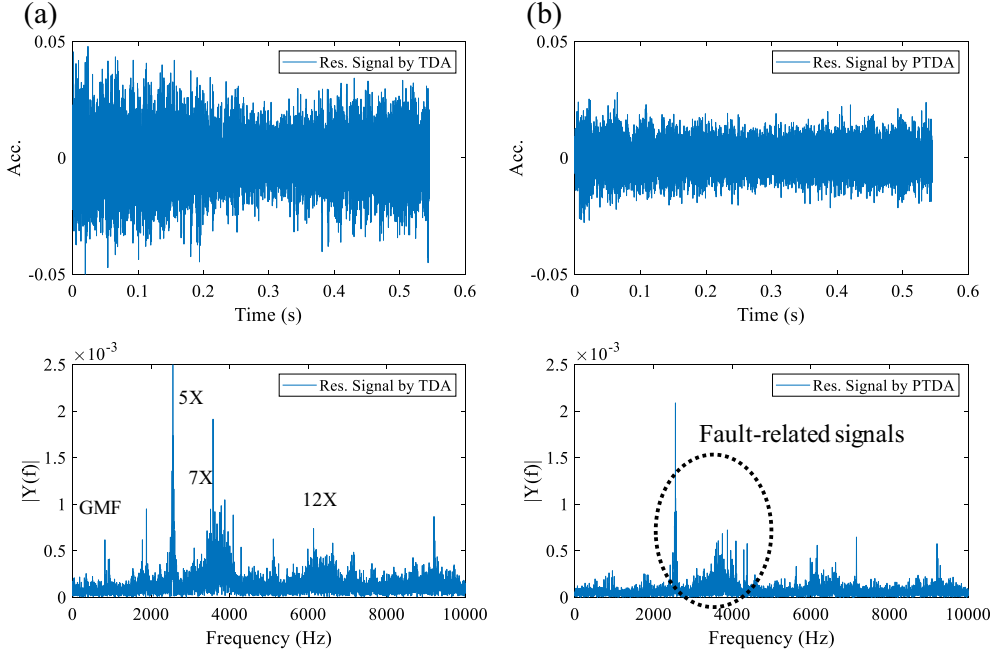


**Fig. 11.** Residual signals in the fault condition using (a) TDA and (b) PTDA.

calculated health features for 19 cycles under both normal and fault conditions. From Fig. 12(a) and (b), the fault detection performances of the extracted raw signals and residual signals with the TDA method were similar. Again, we found that the residual signals from the TDA method could not highlight the fault-related signals. However, as shown in Fig. 12(c), we did find that the fault detection performance was much improved based on the two health features after applying the proposed PTDA method.  $RMS_{res}$  and  $Entropy_{res}$  show about three and two times better results, respectively. The PTDA results are better

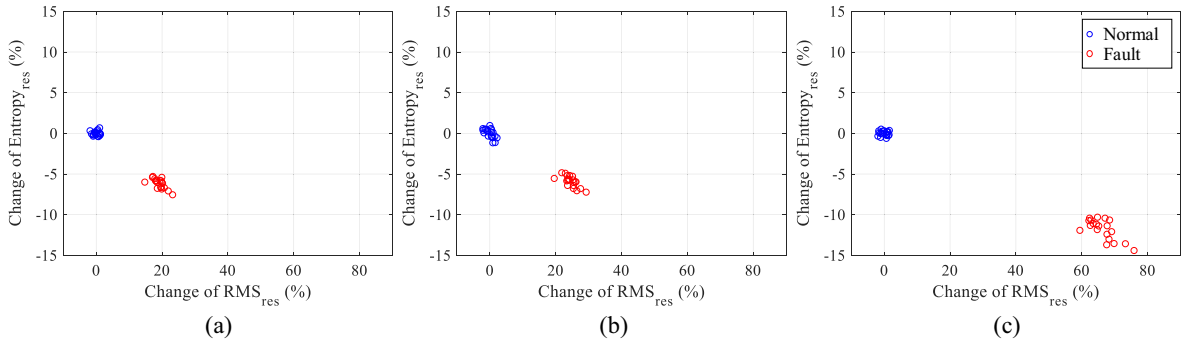


**Fig. 12.** Fault detection results using  $RMS_{res}$  and  $Entropy_{res}$  using (a) raw signals, (b) residual signals with the TDA method, and (c) residual signals with the PTDA method.

because the residual signals from this method have more power of the fault-related signals in the time domain, and the large variation of the magnitude values is found in the frequency domain under the fault condition, as shown in Fig. 11(b).

#### 4.3. Result 2: Arc welding motion

To validate the proposed method for a real case, we operated the industrial robot under an arc welding motion. The arc welding motion profile was provided by Hyundai Robotics. Fig. 13 shows the vibration signal and the angular speed profile at the 4th joint for the arc welding motion. ([The video of the experiment is available in Supplementary material](#)). The vibration signal and the angular speed profile for one cycle of the arc welding motion are shown in Fig. 13(a). Since the working path of the arc welding motion included many via points, the angular speed of the joints showed complex profiles. Fig. 13(b) shows the part of the vibration signal and the angular speed profile including the constant angular speed region. Although the arc welding motion was composed of complicated motions, there was a constant angular speed region due to the trapezoidal shape of the robot angular speed profile [9]. Therefore, we found that the extracted raw signals could be obtained under the constant angular speed region, as shown in Fig. 13(b). Since the extracted raw signals had different phase angles, those signals could not be synchronized. In this case, the time duration of the constant angular speed was 0.14 s and the angular speed was about 4.10 rad/s. The calculated GMF was 618.83 Hz at the constant angular speed using Eq. (3).

Figs. 14 and 15 show extracted raw signals, and deterministic signals found by the TDA method and the PTDA method in normal and fault conditions, respectively. Similar to the previous result, we found that the extracted raw signals have large magnitudes at the GMF and its harmonics from the deterministic signals, as shown in Figs. 14(a) and 15(a). To highlight the fault-related signals, we first derived the deterministic signals using both the TDA and PTDA methods. Figs. 14(b) and 15(b) show the deterministic signals found by the TDA method. Since the extracted raw signals were not entirely synchronized in the time domain, the deterministic signals were not accurate because the magnitudes of the deterministic signals were low at the GMF and its harmonics. Figs. 14(c) and 15(c) show the deterministic signals found by the PTDA method. Likewise, the proposed PTDA method first needs normal signals to find the deterministic signals. Here, the sources of the normal signals are the extracted raw signals from the robot operating in its normal condition. One of the normal signals is presented in

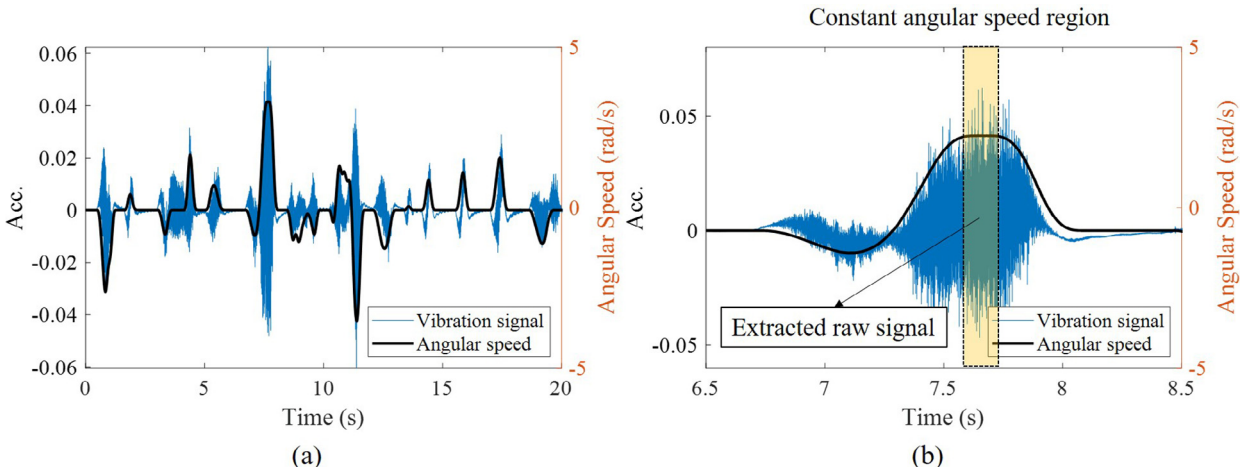


**Fig. 13.** Vibration signal and angular speed profile at the 4th joint under an arc welding motion: (a) one cycle, (b) constant angular speed region.

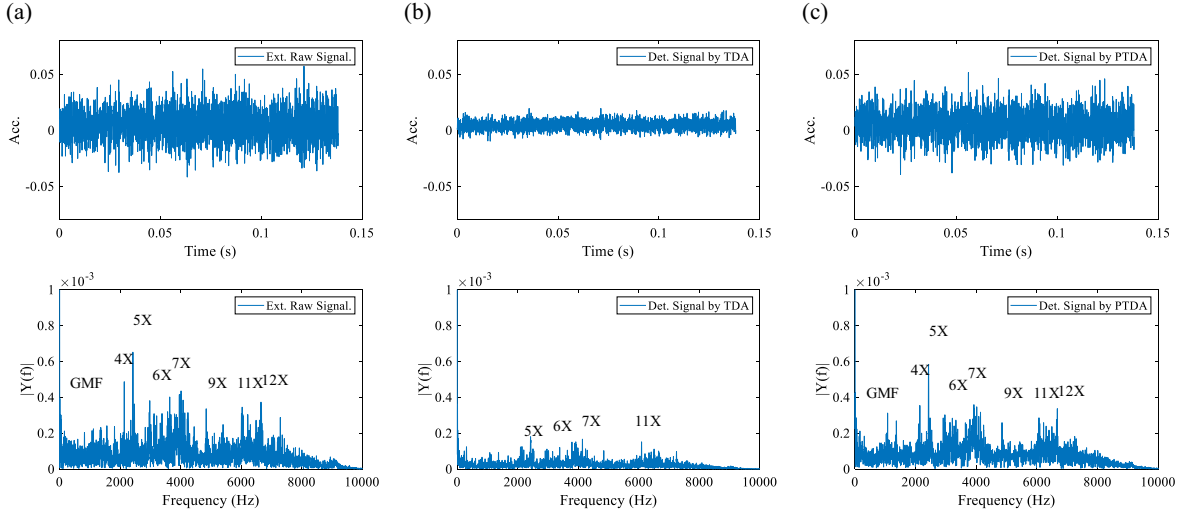


**Fig. 14.** Extracted and deterministic signals in the normal condition: (a) extracted raw signal, (b) deterministic signal found by the TDA method, (c) deterministic signal found by the PTDA method.

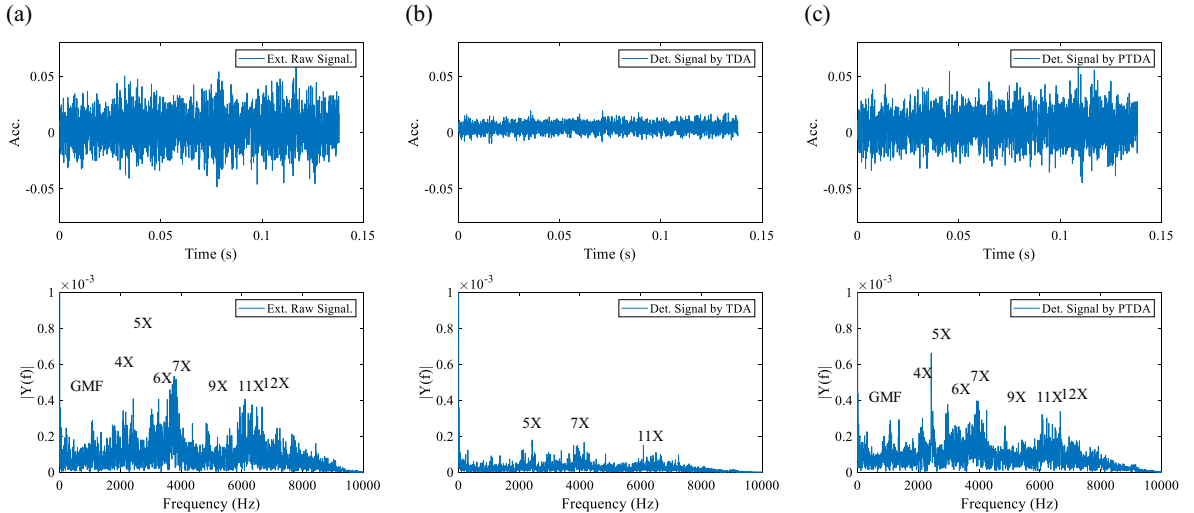


**Fig. 15.** Extracted and deterministic signals in the fault condition: (a) extracted raw signal, (b) deterministic signal found by the TDA method, (c) deterministic signal found by the PTDA method.

**Fig. 14(a).** Unlike the TDA method, we could observe that the estimated deterministic signals found by the PTDA method contained large magnitudes at the GMF and its harmonics in the frequency domain, which represented more accurate deterministic signals than those found with the TDA method.

Figs. 16 and 17 show the residual signals from both the TDA and PTDA methods in the normal and fault conditions. From Figs. 16(a) and 17(a), the residual signals found with the TDA method have large magnitudes at the GMF and its harmonics in the frequency domain. Thus, the residual signals found from TDA could not obtain more sensitive fault-related signals than found in the raw signals. However, as shown in Figs. 16(b) and 17(b), we found that the residual signals derived with the PTDA method have lower magnitudes at the GMF and its harmonics under the arc welding motion. Therefore, the residual signals found with the PTDA method can highlight the fault-related signals, as marked in Fig. 17(b).

Finally, we used the health features,  $RMS_{res}$  and  $Entropy_{res}$ , using the extracted raw signals, the residual signals from the TDA method, and the residual signals from the PTDA method, to see the effectiveness of the proposed method. Fig. 18 shows the rate changes of the calculated health features for 8 cycles of arc welding motion in both normal and fault conditions. As shown in Fig. 18(a), the fault condition showed larger  $Entropy_{res}$  values than the normal condition. Furthermore, Fig. 18(b) shows that the values of  $Entropy_{res}$  for the residual signals found with the TDA method are almost the same for both the

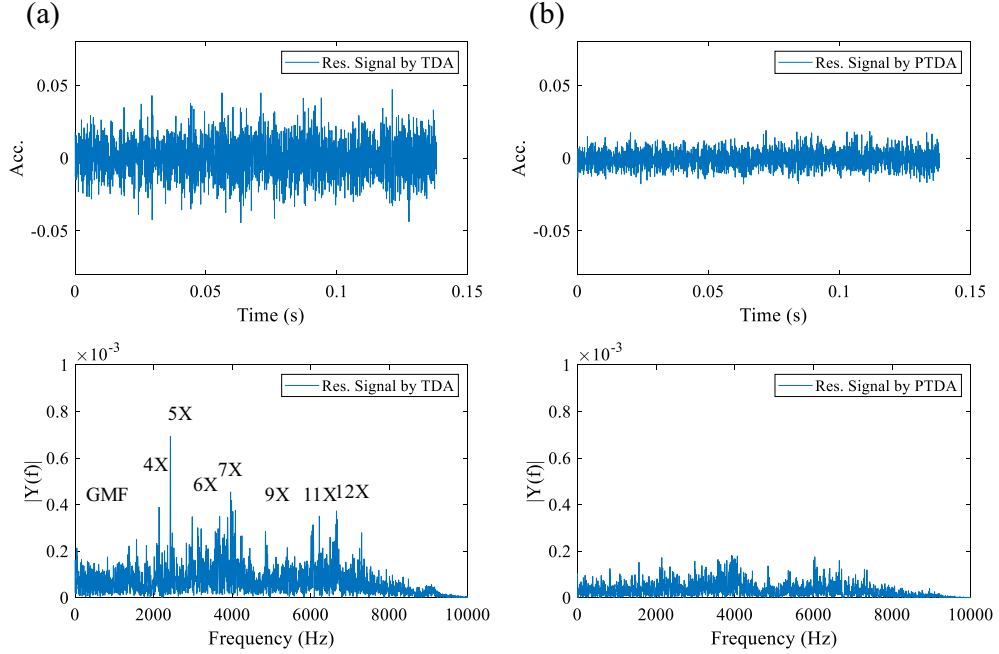


**Fig. 16.** Residual signals in the normal condition using (a) TDA and (b) PTDA.

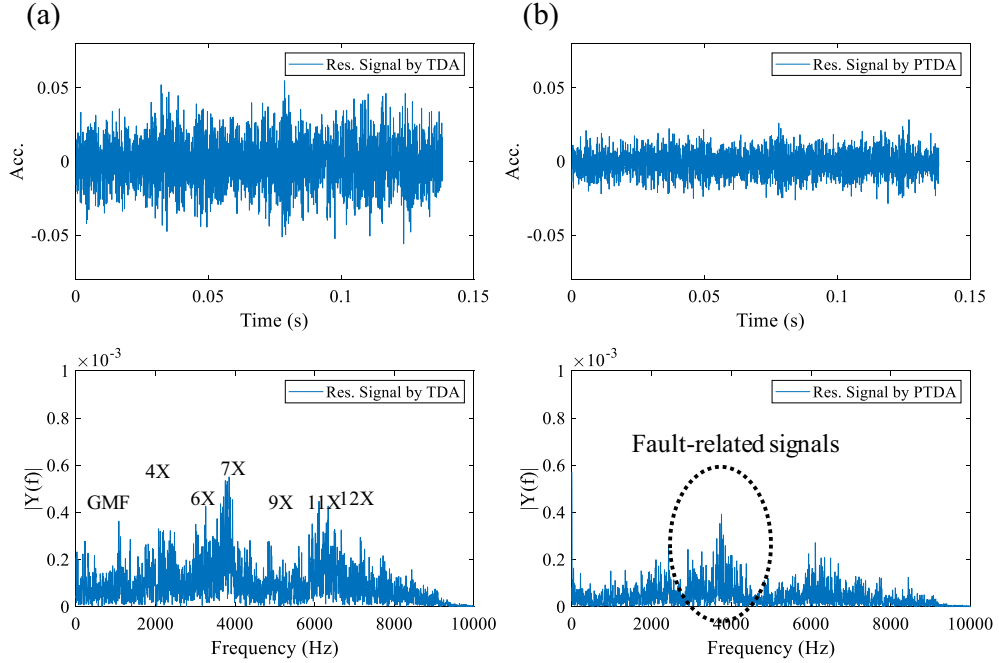


**Fig. 17.** Residual signals in the fault condition using (a) TDA and (b) PTDA.

normal and fault conditions. The variation of the magnitude values in the frequency domain is almost the same for the raw signals and the residual signals from the TDA method in both the normal and fault conditions because of the large magnitude values at the GMF and its harmonics, which are different with those found in Section 4.2. Therefore, we found that  $Entropy_{res}$  could not well quantify the fault severity in either case. Meanwhile, the proposed PTDA method was able to derive residual signals accurately in the frequency domain, as shown in Figs. 16(b) and 17(b). Therefore, as shown in Fig. 18(c), we found

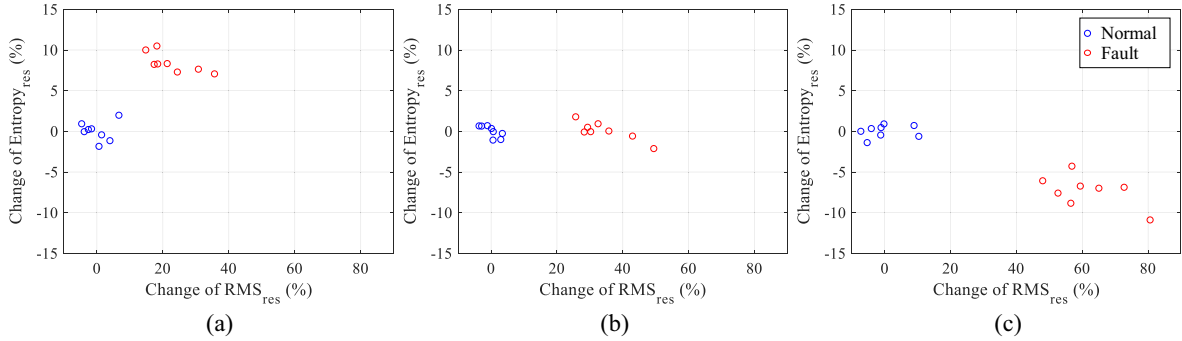


**Fig. 18.** Fault detection results using  $RMS_{res}$  and  $Entropy_{res}$  using (a) raw signals, (b) residual signals found with the TDA method, and (c) residual signals found with the PTDA method.

that  $Entropy_{res}$  could differentiate between the normal and fault conditions. In addition,  $RMS_{res}$  could be more sensitive to the fault than both the extracted raw signals and the residual signals found with the TDA method. This section reveals that the proposed PTDA method also works under the complicated job tasks found for industrial robots in real-world settings.

#### 4.4. Result 3: Spot welding motion

We further validated our proposed method by examining another real-world case involving a spot welding motion. The profile of the spot welding motion was also provided by Hyundai Robotics. Fig. 19 shows the vibration signal and the angular speed profile at the 4th joint for the spot welding motion. ([The video of the experiment is available in Supplementary material](#)). As shown in Fig. 19(a), the movement of the 4th joint represents a small portion of the overall spot welding motion. Nonetheless, the spot welding motion also included the constant angular speed region, as shown in Fig. 19(b). This is due to the trapezoidal shape of the robot's angular speed profile [9]. Therefore, we were able to obtain the extracted raw signals. Further, the extracted raw signals could not be fully synchronized because of the different phase angles. In the constant angular speed region, the output shaft speed is about 1.29 rad/s, and the time length was about 0.48 s. The GMF was computed as 194.87 Hz using Eq. (3).

Figs. 20 and 21 show the extracted raw signals and deterministic signals found by the TDA method and the proposed PTDA method in normal and fault conditions, respectively. As shown in Figs. 20(a) and 21(a), we found that the extracted raw signals have large magnitudes at the GMF and its harmonics due to the excitation of periodic motions, which are the sources of the deterministic signals. Before taking the residual signals for the fault detection, we obtained the deterministic signals with both the TDA and PTDA methods. Figs. 20(b) and 21(b) show the estimated deterministic signals determined through the TDA method. Since the extracted raw signals in the normal condition were not completely synchronized, the TDA method could not derive the deterministic signals properly. The deterministic signals derived from the TDA method included the low magnitudes at the GMF and its harmonics, as shown in Figs. 20(b) and 21(b). Meanwhile, we first need normal signals to obtain deterministic signals via the PTDA method. The normal signals in this case study are the extracted raw signals from the robot operating in its normal condition, as shown in Fig. 20(a). Then, Figs. 20(c) and 21(c) show the deterministic signals estimated through the use of the proposed PTDA method. As shown in Figs. 20(c) and 21(c), we found that the PTDA method could derive appropriate deterministic signals with large magnitudes at the GMF and its harmonics.

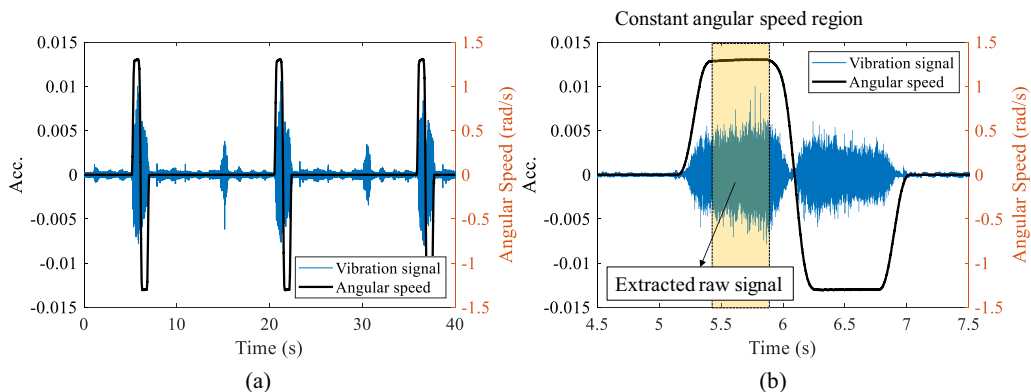


**Fig. 19.** Vibration signal and angular speed profile at the 4th joint under a spot welding motion: (a) three cycle, (b) constant angular speed region.

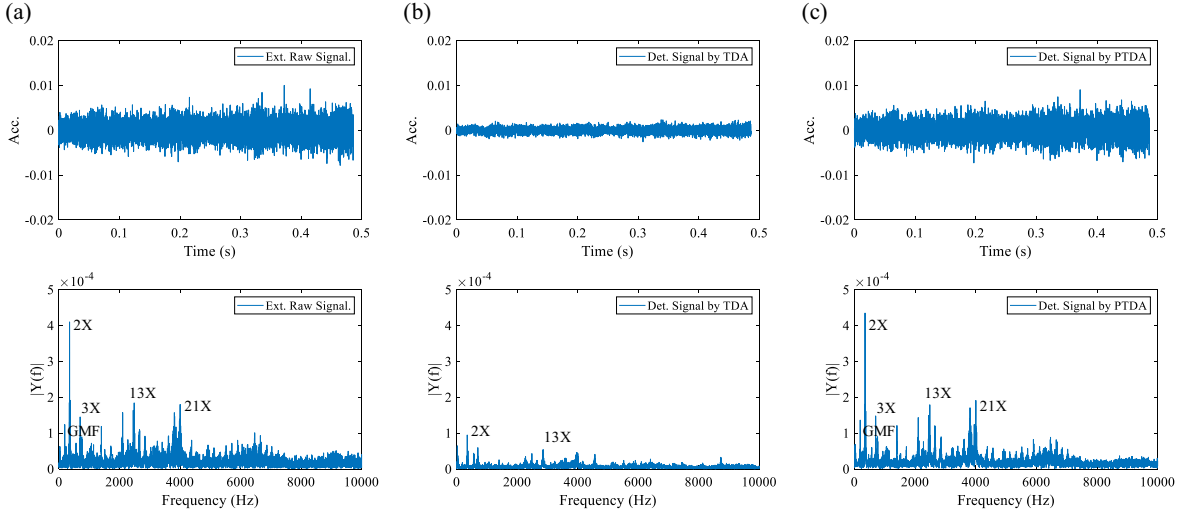


**Fig. 20.** Extracted and deterministic signals in the normal condition: (a) extracted raw signal, (b) deterministic signal found by the TDA method, (c) deterministic signal found by the PTDA method.

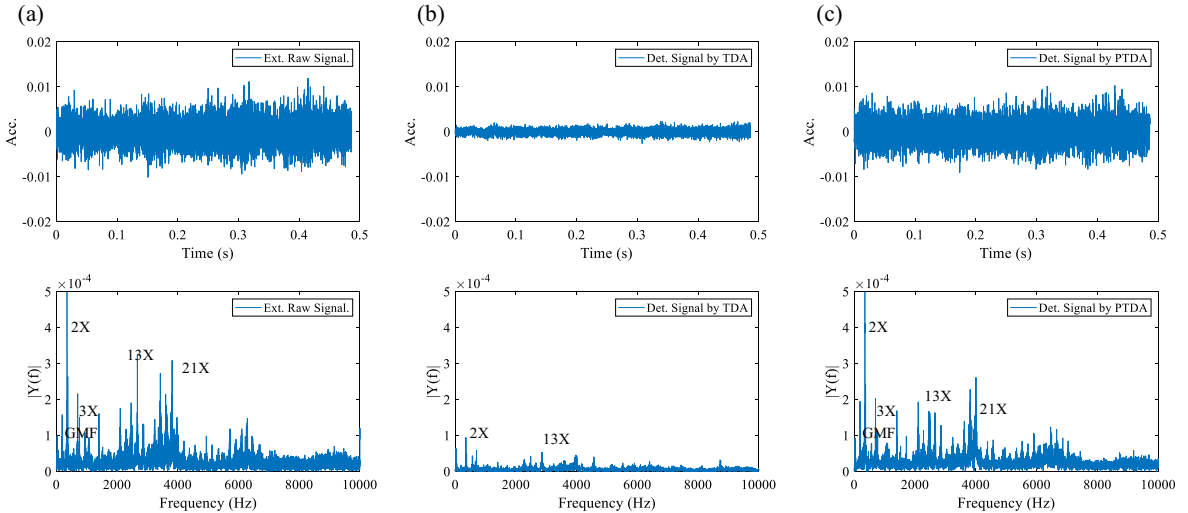


**Fig. 21.** Extracted and deterministic signals in the fault condition: (a) extracted raw signal, (b) deterministic signal found by the TDA method, (c) deterministic signal found by the PTDA method.

Next, we determined the residual signals from the extracted raw signals. Figs. 22 and 23 show the residual signals obtained by the TDA and PTDA methods for normal and faulty conditions, respectively. From Figs. 22(a) and 23(a), we found that the residual signals have large magnitudes at the GMF and its harmonics in the frequency domain. In other words, those residual signals still contained the deterministic signals because of the inaccurate deterministic signals derived from the TDA method. However, as shown in Figs. 22(b) and 23(b), the residual signals show lower magnitudes at the GMF and its harmonics in the frequency domain because the PTDA method is able to derive appropriate deterministic signals by considering the phase angle in the frequency domain. Using this information, the fault-related signals can be highlighted at the residual signals, as marked in Fig. 23(b).

To check the performance of the proposed method, we calculated the health features,  $RMS_{res}$  and  $Entropy_{res}$ , using the extracted raw signals, the residual signals from the TDA method, and the residual signals from the PTDA method. Fig. 24 shows the rate changes of the calculated health features for 9 cycles of the spot welding motion in both normal and fault conditions. As shown in Fig. 24(a) and (b), the fault detection performances of the extracted raw signals and residual signals with the TDA method were similar. A comparison of the two results revealed that the fault-related signals did not appear in the residual signals determined with the TDA method. Meanwhile, as shown in Fig. 24(c), we found that the proposed PTDA

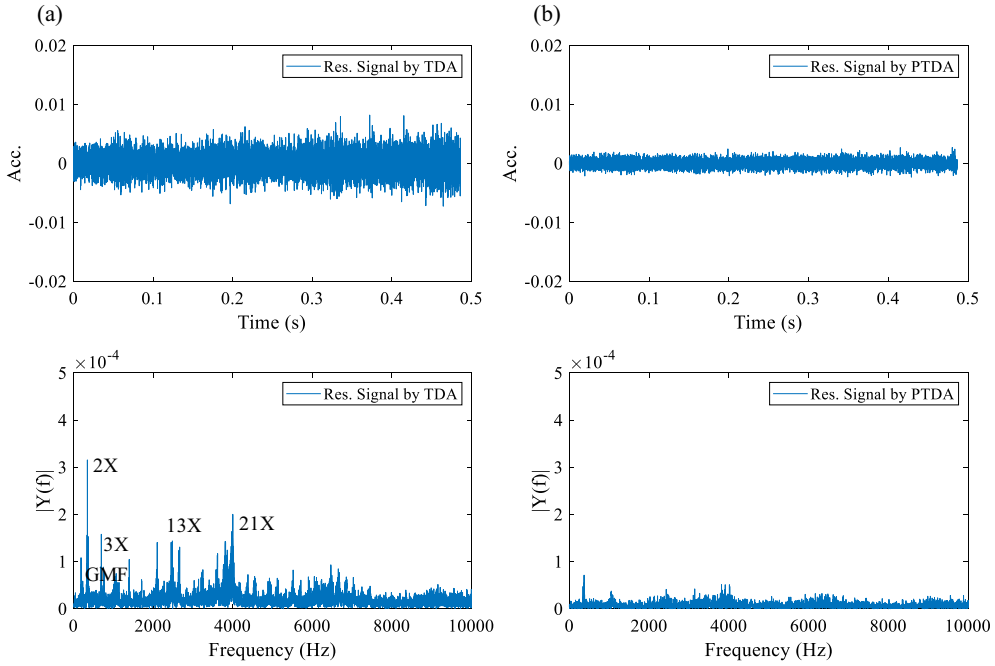


**Fig. 22.** Residual signals in the normal condition using (a) TDA and (b) PTDA.

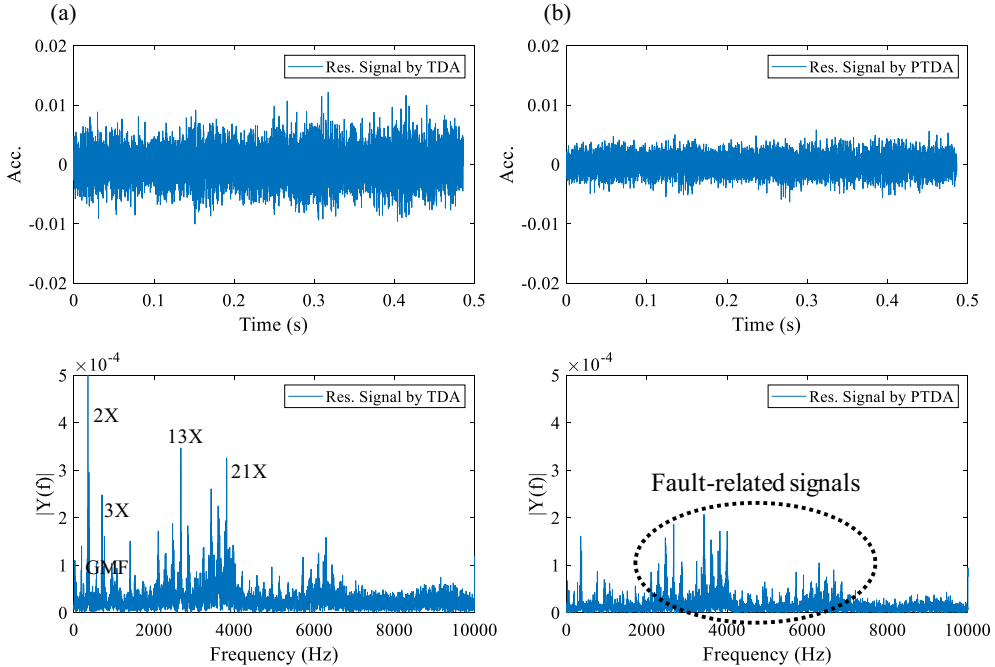


**Fig. 23.** Residual signals in the fault condition using (a) TDA and (b) PTDA.

method improved the fault detection performance based on the two health features. Both  $RMS_{res}$  and  $Entropy_{res}$  determined from the PTDA method were more sensitive to the fault than both the extracted raw signals and the residual signals found with the TDA method. These results further suggest that our proposed PTDA method can detect faults of the industrial robots in real manufacturing lines.

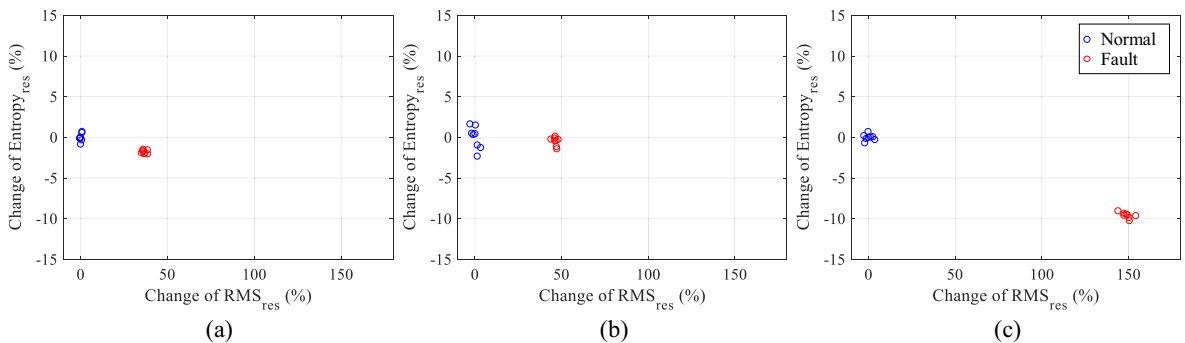


**Fig. 24.** Fault detection results using  $RMS_{res}$  and  $Entropy_{res}$  using (a) raw signals, (b) residual signals found with the TDA method, and (c) residual signals found with the PTDA method.

## 5. Conclusion

In this study, we proposed a new, phase-based time domain averaging (PTDA) method for fault detection of gearboxes used in industrial robots. The proposed method could accurately estimate the deterministic signals from measured signals with different phase angles. In the proposed method, first, the vibration signals were extracted for the constant angular speed region. Then, the deterministic signals were estimated using the PTDA method. The estimated signals included the deterministic signals, such as the GMF and its harmonics in the frequency domain. By considering the phase angle of the vibration signals, the estimated deterministic signals found by the PTDA method could be synchronized with the extracted raw signals. Next, the residual signals could be directly obtained by subtracting the estimated deterministic signals from the extracted raw signals. The residual signals in the normal condition usually consist of noise signals. Meanwhile, the residual signals in the fault condition contain both the noise signals and fault-related signals. Thus, fault severity in the residual signal was quantified using two health features,  $RMS_{res}$  and  $Entropy_{res}$ . The proposed method was demonstrated using a 6-DOF industrial robot test-bed under three job tasks: a single rotating motion, an arc welding motion, and a spot welding motion that allowed consideration of the complex motions of a typical industrial robot. We found that the proposed PTDA method shows better fault detection performance than raw signals and residual signals that use the TDA method for three job tasks. However, the proposed method was developed under an assumption of constant angular speed conditions, and would not be applicable when an industrial robot does not have constant angular speed regions. Therefore, future study should include an extension of the proposed fault detection method to examine variable-speed conditions.

## Declaration of Competing Interest

The authors declare that they have no known competing financial interests or personal relationships that could have appeared to influence the work reported in this paper.

## Acknowledgement

This research was supported by the Basic Research Lab Program through the National Research Foundation of Korea (NRF) funded by the MSIT (2018R1A4A1059976). This research was also supported by a grant from Hyundai Robotics.

## Appendix A. Supplementary data

Supplementary data to this article can be found online at <https://doi.org/10.1016/j.ymssp.2019.106544>.

## References

- [1] K. Eguchi, Q. Wu, Y. Liu, C. Wu, T. Chen, An overview of current situations of robot industry development, *ITM Web Conf.* 17 (2018).
- [2] J.J. Craig, *Introduction to robotics: mechanics and control*, Pearson/Prentice Hall Upper Saddle River, NJ, USA, 2005.
- [3] IFR World robotics [online]. Retrieved from [https://ifr.org/downloads/press2018/Executive\\_Summary\\_WR\\_2018\\_Industrial\\_Robots.pdf](https://ifr.org/downloads/press2018/Executive_Summary_WR_2018_Industrial_Robots.pdf).
- [4] S. Wang, X. Zhang, W. Xu, A. Liu, Z. Zhou, D.T. Pham, Energy-efficient concurrent assessment of industrial robot operation based on association rules in manufacturing, in: *Proceedings of the 2018 IEEE 15th International Conference on Networking, Sensing and Control (ICNSC)*, 2018, pp. 1–6.
- [5] D. Kravets, “Jan. 25 1979: Robot kills human,” in *Wired*, ed, 2010.
- [6] B. Freyermuth, An approach to model based fault diagnosis of industrial robots, in: *Proceedings of the 1991 IEEE International Conference on Robotics and Automation*, 1991, pp. 1350–1356.
- [7] L.M. Capisani, A. Ferrara, A. Ferreira, L. Fridman, Higher Order Sliding Mode observers for actuator faults Diagnosis in robot manipulators, in: *Proceedings of the 2010 IEEE International Symposium on Industrial Electronics*, 2010, pp. 2103–2108.
- [8] C. Yang, Y. Jiang, W. He, J. Na, Z. Li, B. Xu, Adaptive parameter estimation and control design for robot manipulators with finite-time convergence, *IEEE Trans. Ind. Electron.* 65 (10) (2018) 8112–8123.

- [9] M.-C. Pan, H. Van Brussel, P. Sas, Intelligent joint fault diagnosis of industrial robots, *Mech. Syst. Sig. Process.* 12 (4) (1998) 571–588.
- [10] A.A. Jaber, R. Bicker, Industrial robot backlash fault diagnosis based on discrete wavelet transform and artificial neural network, *Am. J. Mech. Eng.* 4 (1) (2016) 21–31.
- [11] A. Datta, C. Mavroidis, J. Krishnasamy, M. Hosek, Neural netwrk based fault diagnostics of industrial robots using wavelt multi-resolution analysis, in: *Proceedings of the 2007 American Control Conference*, 2007, pp. 1858–1863.
- [12] G. Qiao, B.A. Weiss, Quick health assessment for industrial robot health degradation and the supporting advanced sensing development, *J. Manuf. Syst.* 48 (2018) 51–59.
- [13] A.W.K. To, G. Paul, D. Liu, A comprehensive approach to real-time fault diagnosis during automatic grit-blasting operation by autonomous industrial robots, *Rob. Comput. Integrat. Manuf.* 49 (2018) 13–23.
- [14] V. Sharma, A. Parey, Frequency domain averaging based experimental evaluation of gear fault without tachometer for fluctuating speed conditions, *Mech. Syst. Sig. Process.* 85 (2017) 278–295.
- [15] J.M. Ha, B.D. Youn, H. Oh, B. Han, Y. Jung, J. Park, Autocorrelation-based time synchronous averaging for condition monitoring of planetary gearboxes in wind turbines, *Mech. Syst. Sig. Process.* 70–71 (2016) 161–175.
- [16] J. Park, M. Hamadache, J.M. Ha, Y. Kim, K. Na, B.D. Youn, A positive energy residual (PER) based planetary gear fault detection method under variable speed conditions, *Mech. Syst. Sig. Process.* 117 (2019) 347–360.
- [17] J.P. Salameh, S. Cauet, E. Etien, A. Sakout, L. Rambault, Gearbox condition monitoring in wind turbines: A review, *Mech. Syst. Sig. Process.* 111 (2018) 251–264.
- [18] M. Ruiz et al., Wind turbine fault detection and classification by means of image texture analysis, *Mech. Syst. Sig. Process.* 107 (2018) 149–167.
- [19] J.M. Ha, J. Park, K. Na, Y. Kim, B.D. Youn, Toothwise fault identification for a planetary gearbox based on a health data map, *IEEE Trans. Ind. Electron.* 65 (7) (2018) 5903–5912.
- [20] J. Park, J.M. Ha, H. Oh, B.D. Youn, J.-H. Choi, N.H. Kim, Model-based fault diagnosis of a planetary gear: A novel approach using transmission error, *IEEE Trans. Reliab.* 65 (4) (2016) 1830–1841.
- [21] J. Park, Y. Kim, K. Na, B.D. Youn, Variance of energy residual (VER): An efficient method for planetary gear fault detection under variable-speed conditions, *J. Sound Vib.* 453 (2019) 253–267.
- [22] R. Randall, N. Sawalhi, M. Coats, A comparison of methods for separation of deterministic and random signals, *Int. J. Condition Monit.* 1 (1) (2011) 11–19.
- [23] X. Xu, J. Lin, C. Yan, Adaptive determination of fundamental frequency for direct time-domain averaging, *Measurement* 124 (2018) 351–358.
- [24] W. Wang, P. McFadden, Application of wavelets to gearbox vibration signals for fault detection, *J. Sound Vib.* 192 (5) (1996) 927–939.
- [25] W. Wang, Early detection of gear tooth cracking using the resonance demodulation technique, *Mech. Syst. Sig. Process.* 15 (5) (2001) 887–903.
- [26] L. Pan, T. Gao, F. Xu, L. Zhang, Enhanced robust motion tracking control for 6 degree-of-freedom industrial assembly robot with disturbance adaption, *Int. J. Control Autom. Syst.* 16 (2) (2018) 921–928.
- [27] S. Kumra, R. Saxena, S. Mehta, Design and development of 6-DOF robotic arm controlled by Man Machine Interface, in: *Proceedings of the 2012 IEEE International Conference on Computational Intelligence & Computing Research*, 2012, p. 1.
- [28] A.A. Jaber, *Design of an Intelligent Embedded System for Condition Monitoring of an Industrial Robot*, Springer, 2016.
- [29] K. Wu, C. Krewet, B. Kuhlenkötter, Dynamic performance of industrial robot in corner path with CNC controller, *Rob. Comput. Integrat. Manuf.* 54 (2018) 156–161.
- [30] X. Yin, L. Pan, Direct adaptive robust tracking control for 6 DOF industrial robot with enhanced accuracy, *ISA Trans.* 72 (2018) 178–184.
- [31] X. Liu, X. Wu, C. Liu, T. Liu, Research on condition monitoring of speed reducer of industrial robot with acoustic emission, *Trans. Can. Soc. Mech. Eng.* 40 (5) (2016) 1041–1049.
- [32] W.-S. Lin, Y.-P. Shih, J.-J. Lee, Design of a two-stage cycloidal gear reducer with tooth modifications, *Mech. Mach. Theory* 79 (2014) 184–197.
- [33] H. Endo, R. Randall, Enhancement of autoregressive model based gear tooth fault detection technique by the use of minimum entropy deconvolution filter, *Mech. Syst. Sig. Process.* 21 (2) (2007) 906–919.
- [34] Y. Lei, J. Lin, M.J. Zuo, Z. He, Condition monitoring and fault diagnosis of planetary gearboxes: A review, *Measurement* 48 (2014) 292–305.
- [35] A.V. Oppenheim, *Discrete-Time Signal Processing*, Pearson Education India, 1999.
- [36] V. Sharma, A. Parey, A review of gear fault diagnosis using various condition indicators, *Procedia Eng.* 144 (2016) 253–263.
- [37] G. Cheng, X. Chen, H. Li, P. Li, H. Liu, Study on planetary gear fault diagnosis based on entropy feature fusion of ensemble empirical mode decomposition, *Measurement* 91 (2016) 140–154.
- [38] C.M. Bishop, *Pattern recognition and machine learning*, Spring-Verlag New York, Inc., 2006.
- [39] J. Mortimer, Adhesive bonding of car body parts by industrial robot, *Ind. Robot: Int. J.* 31 (5) (2004) 423–428.